Self-similarity of Images in the Fourier Domain, with Applications to MRI

G.S. Mayer[1], Edward R. Vrscay[1], M.L. Lauzon[2], B.G. Goodyear[2,3], and J.R. Mitchell[2]

[1] Department of Applied Mathematics, Faculty of Mathematics, University of Waterloo, Waterloo, Ontario, Canada N2L 3G1
[2] The Seaman Family MR Research Centre, Calgary, Alberta, Canada, T2N 2T9
[3] The Department of Radiology, University of Calgary, Alberta, Canada, T2N 1N4
{gsmayer,ervrscay}@uwaterloo.ca

Abstract. Results presented in this paper represent part of an ongoing research programme dedicated to the resolution enhancement of Fourier domain magnetic resonance (MR) data. Here we explore the use of self-similarity methods that may aid in frequency extrapolation of such data. To this end, we present analytical and empirical results demonstrating the self similarity of complex, Fourier domain MR data.

1 Introduction

In a previous ICIAR paper [15], we showed how resolution enhancement could be accomplished by means of a fractal-based method over complex-valued Fourier data with compact support $X \subset \mathbb{R}$. Our method of "iterated Fourier transform systems" (IFTS) is the Fourier domain counterpart of the fractal-based method of "iterated function systems with greyscale maps" (IFSM) in the spatial domain [7]. The action of an IFTS operator $\hat{M}$ on Fourier data $U(\omega)$ produces frequency-expanded and phase-ramped, range-distorted copies of U. We then showed how this method could perform *frequency extrapolation* as follows. Suppose that the raw MR data is given by the complex-valued Fourier data $U_0(\omega)$ with support $\omega \in \Omega_0 = [-\omega_0, \omega_0]$. Furthermore assume that U_0 is the bandlimited version of the "true" Fourier transform $U(\omega),\ \omega \in \mathbb{R}$. We first solve an inverse problem by determining a contractive IFTS operator $\hat{M}$ to minimizes the *collage distance* $\|U_0 - \hat{M}U_0\|$. Because of the frequency-expansive nature of the operator $\hat{M}$, the function $U_1 = \hat{M}U_0$ is supported over a *larger* interval $\Omega_1 = [-\omega_1, \omega_1]$, where $\omega_1 = A\omega_0$ and $A > 1$. As such, higher frequency components of U outside the interval Ω_0 are estimated, thereby achieving higher spatial domain resolution.

This paper explores the use of self-similarity methods on frequency domain data. A major motivation for our work is provided by recent work [2] showing that images are, in general, affinely self-similar locally: Given a "range block" $u(R_i)$ of an image, there are generally a number of "domain blocks" $u(D_j)$ that can approximate it well under the action of affine greyscale transforms. This spatial domain self-similarity is dramatically demonstrated when errors of approximation are plotted for all domain-range pairings.

A. Campilho and M. Kamel (Eds.): ICIAR 2008, LNCS 5112, pp. 43–52, 2008.

Here we demonstrate that such self-similarity is also exhibited by subblocks of Fourier data. The underlying explanation for this block-based self-similarity is that a connection can be made between the well-known result of autoregressive (AR) correlation coefficients and block-based fractal coding. This justifies block-based fractal coding in the complex Fourier domain, which we then employ for the purpose of frequency extrapolation.

To this end, we show that discrete functions of the form,

$$s(m) = \sum_{n=1}^{N} c(n) e^{\sigma_n m}, \qquad m \in \mathbb{Z}, \quad c_n, \sigma_n \in \mathbb{C} \tag{1}$$

are locally self-similar. Variables N (the number of terms in the summation), and σ_n (an arbitrary complex number), have specific physical interpretations when Eq (1) is placed in the context of a given application. Functions of the form Eq (1) are found in many applications, but here we consider their use in magnetic resonance (MR). Eq (1) has been used to model the measured MR data in order to improve the image reconstruction process and to reduce artifacts [9].

Block-based fractal coding in the wavelet domain is a rather standard procedure [19]. To the best of our knowledge, however, there has been little analysis to date on the use of fractal-based methods to analyze or process Fourier data. This paper and our previous manuscript [15] represent work in this direction.

2 MRI and Some One-Dimensional MRI Data Models

Here, we outline general spatial and frequency domain models for MRI data, where the raw data is a Fourier spectrum of the desired image. For simplicity of notation and presentation, we first consider one-dimensional MRI procedures.

The MR scanner responds to the *proton density* of the object, to be denoted as $\rho(x)$, and produces a complex-valued signal $s(k)$ of the real-valued frequency parameter k. The relation between $s(k)$ and the proton density function $\rho(x)$ may be expressed as [11,13,10]:

$$s(k) = \int_{-\infty}^{+\infty} \rho(x) \exp(-i2\pi kx) dx, \qquad k \in \mathbb{R}. \tag{2}$$

In other words, $s(k)$ is related to $\rho(x)$ via the Fourier transform [10]. If $s(k)$ is known $\forall\ k \in \mathbb{R}$, then $\rho(x)$ may be found by using the inverse Fourier transform of $s(k)$. In practice however, the true proton density, $\rho(x)$, cannot be obtained exactly, and must be estimated. Ultimately, reconstruction yields only approximations to $\rho(x)$ with finite spatial resolution.

Standard MRI Data Models

Several approaches to modeling MR data based on *a priori* knowledge of the acquisition process have been proposed to improve image reconstruction. In the *boxcar model* [9], $\rho(x)$ is represented as a sum of N_C indicator functions:

$$\rho_{N_C}(x) = \sum_{m=1}^{N_C} c_m W_m(x), \quad W_m(x) = \begin{cases} 1, \left|\frac{x-p_m}{q_m}\right| \leq \frac{1}{2} \\ 0, \left|\frac{x-p_m}{q_m}\right| > \frac{1}{2} \end{cases}. \tag{3}$$

Variables p_m and q_m are the respective centers and widths of each indicator function. Substitution into Eq (2) yields:

$$s_{N_C}(k) = \frac{1}{\pi k} \sum_{m=1}^{N_C} c_m \sin(\pi q_m k) e^{-2\pi i k p_m}. \tag{4}$$

Multiplication by $-2\pi ik$ and sampling converts $s_{N_C}(k)$ into the form of Eq (1):

$$\hat{s}_{N_C}(n) = -2\pi ik s_{N_C}(n) = \sum_{m=1}^{2N_C} d_m e^{-2\pi i n r_m}, \ n = 0, 1, 2, \ldots, N_S - 1. \tag{5}$$

where the number of samples is N_S, and

$$r_m = \begin{cases} q_m/2 - p_m, m = 1, 2, \ldots, N_C \\ q_m/2 + p_m, m = N_C + 1, N_C + 2, \ldots, 2N_C \end{cases}$$
$$d_m = \begin{cases} c_m, & m = 1, 2, \ldots, N_C \\ c_{m-N_C}, m = N_C + 1, N_C + 2, \ldots, 2N_C \end{cases}$$

It has been shown that discrete signals in the form of Eq (5) obey [17,20]:

$$\hat{s}_{N_C}(n) = -\sum_{m=1}^{2N_C} a_m \hat{s}(n-m), \quad n = 2N_C, 2N_C + 1, \ldots, N_s - 1. \tag{6}$$

This result is a consequence of Prony's method [17], and the coefficients $a_m \in \mathbb{C}$ are known as the *autoregressive* (AR) coefficients [14]. This model of the MR data provides us with relations for fractal parameters that are later introduced.

2.1 Self-similarity of the One-Dimensional MR Signal

Many of the fractal-based methods developed thus far utilize local self-similarities between different regions of real *spatial domain* images. For fractal-based methods to be effective on complex *Fourier domain* data we require that this data be self-similar, and the extent to which it is locally self-similar has not, to the best of our knowledge, been explored to date.

In order to initiate a discussion of the self-similarity of Fourier data, we first consider the complex, discrete signal, $s(n) \in l^2(\mathbb{C}), \quad n = 0, 1, 2, \ldots N_S - 1$. Then define a partitioning of $s(n)$ into domain and range vectors (or *blocks*) and affine transforms that operate on these blocks. The last N_P values of $s(n)$ will constitute the range block, $\mathbf{r}$:

$$\mathbf{r} = [s(N_S - N_P), s(N_S - N_P + 1), \ldots, s(N_S - 1)]. \tag{7}$$

The domain vectors are constructed by partitioning $s(n)$ into $N_{DB} = N_S - N_P$ *overlapping* domain blocks:

$$\begin{aligned}\mathbf{d}_m = [s(p), s(p+1), s(p+2), \ldots, s(p+N_P-1)],\\ p = N_S - N_P - m,\\ m = 1, 2, \ldots, N_{DB}.\end{aligned}$$

The set of all domain blocks, $D = \{\mathbf{d}_m \in \mathbb{C}^{N_P} |\ m = 1, 2, \ldots, N_{DB}\}$, comprises the *domain pool*. Fractal-based algorithms typically use affine transforms to search for similarities between the intensities of range and domain blocks. If for a given range block, we can find an affine transform T, and domain block d_m, such that $\mathbf{r} \approx T\mathbf{d}_m$, then the given data possesses some degree of *self-similarity*.

Transforming the intensities of a single domain block by $\alpha_m, \beta_m \in \mathbb{C}$ defines a simple transform to approximate $\mathbf{r}$:

$$\mathbf{r} \approx T_1(\mathbf{d}_m) = \alpha_m \mathbf{d}_m + \beta_m. \tag{8}$$

The subscript of the operator T denotes that a *single* domain block is being used to approximate $\mathbf{r}$. The complex parameters α_m and β_m may be chosen by minimizing the l^2 (vector) norm, Δ_m of the difference between $\mathbf{r} \in \mathbb{C}^{N_P}$ and each affinely-transformed domain vector[1]:

$$\Delta_m = \sqrt{\frac{1}{N_P} \sum_{n=1}^{N_P} \left|\mathbf{r}(n) - [\alpha_m \mathbf{d}_m(n) + \beta_m]\right|^2}. \tag{9}$$

Another fractal operator uses a set of N_{PB} domain (or *parent*) blocks instead of a single $\mathbf{d}_m$ to approximate $\mathbf{r}$ [1]:

$$\mathbf{r} \approx T_{N_{PB}}(D_\Lambda) = \beta_m + \sum_{m \in \Lambda} \alpha_m \mathbf{d}_m. \tag{10}$$

The vector set $D_\Lambda \subset D$ denotes a set of N_{PB} parents[2] chosen from the domain pool, D. With a multi-parent approach, the parameters α_m may be chosen to combine the domain blocks in a number of ways [1,3,5].

Relation between Fractal and Autoregressive Based Methods

In this section, we make a connection between fractal and AR equations to demonstrate certain self-similar properties of one-dimensional MR data. Combining Eq (7) for the range block $\mathbf{r}$ with Eq (6), we obtain (Appendix):

$$\mathbf{r} = -\sum_{m=1}^{2N_C} a_m \mathbf{d}_m \tag{11}$$

[1] The parameter Δ is simply the root mean squared error between $\mathbf{r}(n)$ and its approximation, and is referred to in the fractal literature as the *collage error*.

[2] For example, the N_{PB} parents that have the lowest collage errors, according to Eq (9) may be chosen.

Comparing Eqs (10) and (11), several key observations can be made. First, by allowing $\beta = 0$ and using an appropriate set for Λ, we obtain

$$\alpha_m = -a_m, \quad m = 1, 2, 3, \ldots, 2N_C,$$

so that the approximation in Eq (10) becomes an equality. That is, multi-parent fractal operators acting on signals of the form Eq (1) can produce $\mathbf{r}$ *exactly* without the need for a β term[3]. Thus, using the boxcar model [9] *one dimensional MR signals are self similar* upon multiplication of the signal by $-2\pi ik$.

Having established a connection between fractal coding and AR modeling, new results could be explored with AR modeling that describe mathematical and physical properties of the fractal parameters α and β. This connection enables a relationship between, for example, α and physical parameters (in this case, p_m and q_m of Eq (3)) through Prony or AR modeling [12]. Deriving such connections is, however, beyond the scope of this paper.

Eq (11) represents a theoretical derivation for *one*-dimensional complex signals. Although mathematical extensions of Prony and AR methods to two dimensions has been made (see for example [4,18]), our research into the extension of the mathematical connection between fractal and AR theory to two dimensions is in progress. Rather, the next section explores the *empirical* evidence that two dimensional complex MRI Fourier data can demonstrate self-similarity.

3 Two Dimensional Fractal Coding of MRI Data

In this section, we present a preliminary analysis of the self-similar properties of two dimensional MRI data. We explore the self-similarity of MR data, using two-dimensional blocks, in the Fourier domain, employing single and multiple parent transforms, with MRI data taken from two different MR imaging systems.

Photographs of MR "phantoms", constructed with plexiglass sheets mounted on 2 cm diameter cylindrical Teflon bases are shown in Figs 1(a) and 1(b). Figs 1(c) and 1(d) show MR images[4] of these phantoms immersed in water. Fig 1(c) has dimensions 256×256, Fig 1(d) has dimensions 512×512. Figs 1(e), (f) display the respective k-space real components between [-2.5e-4,+2.5e+4]. Figs 1(g) and (h) display the respective k-space magnitudes and the relative amplitudes at the origin and at high frequencies.

Fig 2 shows data[5] from a 30 slice data set of a human volunteer. Each slice is a complex k-space data set with dimensions 128×128. The (a) spatial domain magnitude, (b) k-space real component, and (c) k-space magnitude are displayed. Each image was individually normalized by their respective l^2 norms.

[3] Admittedly, we have considered the noiseless case, and would not expect that the collage error would remain zero under the presence of noise.

[4] 11.7 T MRI system (Bruker), using a gradient echo sequence, TR/TE 800/5 ms, FOV 3 cm.

[5] 3.0 T MRI system (General Electric Medical Systems; Waukesha, WI), using a multislice spoiled gradient-recalled echo sequence, FOV 24 cm, slick thickness 4 mm, TR/TE 200/3.1 ms, flip angle 18°.

Collage error probability histograms (CEPH) were constructed from the phantom data. The histograms were made by partitioning the k-space data sets into N_{DB} non-overlapping $N_P \times N_P$ *domain* and *range* blocks. The domain and range block sets were exactly the same. For each range block, all possible domain blocks were compared (with the exception of those domain blocks that were equal to the corresponding range block), using the 2D analog of Eq (9), or *collage error*:

$$\Delta_{p,q} = \sqrt{\frac{1}{N_P^2} \sum_{m,n=1}^{N_P} |\mathbf{r}_p(m,n) - \alpha_q \mathbf{d}_q(m,n) - \beta_q|^2}, \; p,q = 1,2,\ldots,N_{DB}, \; p \neq q \tag{12}$$

A total of $N_{DB} \times (N_{DB} - 1)$ comparisons are made to construct a CEPH. The parameters α_q and β_q are determined using a least-squares fit to $\mathbf{r}_p$. CEPHs calculated using Eq (12) from the phantom and human volunteer data are shown in Figs 3 and 4, using $N_P = 4$.

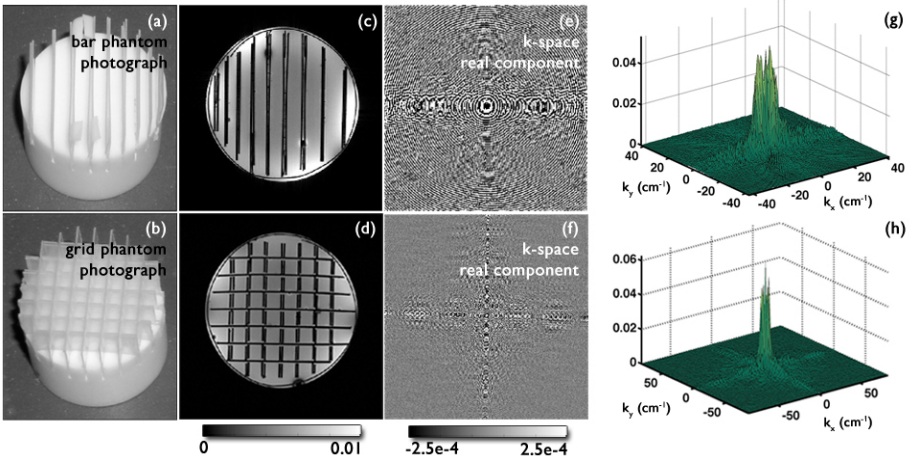

Fig. 1. Photographs of the (a) "bar" and (b) "grid" phantoms. (c) and (d) display spatial domain magnitudes. (e) and (f) show the corresponding k-space real component between [-2.5e-4, 2.5e-4], and (g) and (h) show the k-space magnitude data. Data sets were normalized in l^2.

Complex noise taken from a normal distribution with zero mean and SD 0.005 was added to the normalized human volunteer data and the normalized phantom data. The corresponding CEPHs and SD histograms from the phantom and human volunteer data are displayed in Figs 3 and 4.

In all of the CEPHs (Figs 3, 4, 5), the additive noise moved the distributions away from zero to a new distribution centered near 0.005. This effect is not surprising, as the CEPHs of *pure* noise is centered on its SD [8]. We also see that the pure k-space data is more self-similar than the data obtained after adding

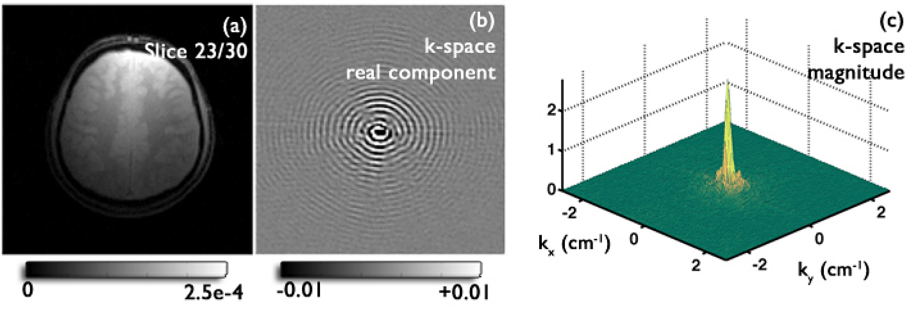

Fig. 2. One slice from the 30 slice human volunteer data. (a) displays the magnitude of the spatial domain data, (b) the corresponding k-space real component intensities between -0.01 and +0.01, and (c) shows the k-space data magnitude.

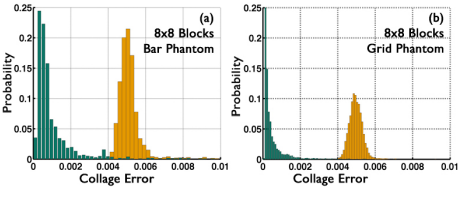

Fig. 3. CEPHs from phantom data using 8×8 blocks (green), and the corresponding histograms with added complex zero mean noise with SD 0.005 (orange)

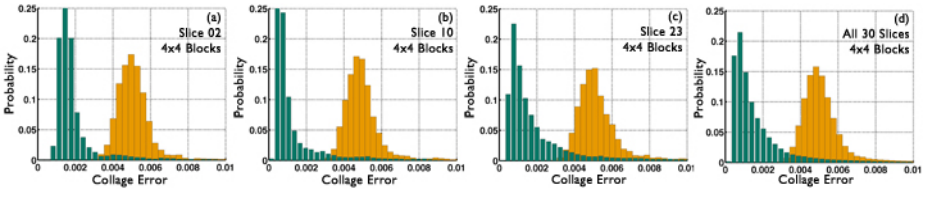

Fig. 4. (a) to (c) human volunteer CEPHs (green) using 4×4 blociks and corresponding CEPHs after noise was added (orange). CEPHs in (d) were calculated from all 30 slices.

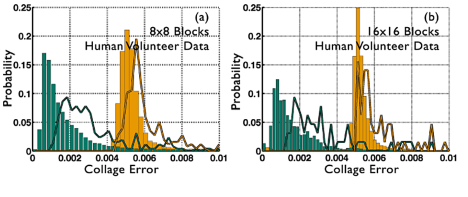

Fig. 5. (a) and (b) human volunteer CEPHs (green) from all 30 slices using different block sizes, and the corresponding CEPHs after noise was added (orange). Green and orange lines correspond to range block SD histograms.

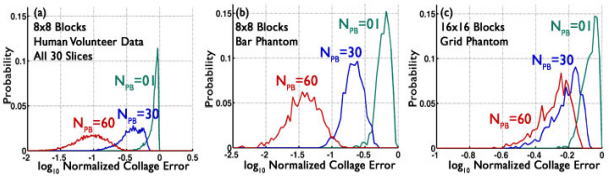

Fig. 6. Normalized multi-parent CEPHs using $N_{PB} = 1, 30$, and 60, from various data sets. Errors are plotted on a $\log_{10}$ scale, and collage errors are normalized by the SD of $\mathbf{r}_p$. Only the N_{PB} blocks for each $\mathbf{r}_p$ with the lowest collage errors were used to calculate the least squares projection onto the N_{PB} blocks.

Table 1. Mean normalized multi-parent collage errors using $N_{PB} = 1, 30$, and 60, from various data sets. Collage errors are normalized by the SD of $\mathbf{r}_p$. Only the N_{PB} blocks for each $\mathbf{r}_p$ with the lowest collage errors were used to calculate the least squares projection onto the N_{PB} blocks. Means are calculated across all range blocks.

N_{PB}	Bar, $N_P = 8$	Grid, $N_P = 16$	Human Volunteer, $N_P = 8$
1	0.6179	0.8505	0.8300
30	0.2234	0.6221	0.3955
60	0.0435	0.5299	0.1028

noise, providing us with evidence that two dimensional k-space data may be self-similar, or at least can be more self-similar with less noise.

The collage errors in Fig 4 were closer to the origin than the SDs. The SDs are simply the collage errors, using Eq (12), with $\alpha_q = 0$. Including the α_q term reduces Δ, further suggesting that k-space data can be self-similar.

CEPHs were also calculated using a *multi-parent* transform. The collage error between the range blocks and the least-squares projection of each range block onto the space spanned by the N_{PB} transformed domain blocks with the lowest collage errors for each range block was calculated. The CEPHs for $N_{PB} = 1, 10$, and 30 are shown in Fig 6. The collage errors were normalized by the SDs of the range blocks, and the errors were plotted on a logarithmic scale. Table 1 shows the means of collage errors plotted in Fig 6. As expected, the collage errors become smaller as more parents are used.

4 Conclusions

This paper represents an important step in our research programme for frequency extrapolation of Fourier domain data using fractal and self-similar based methods. To this end, we investigated the local self-similarity of two classes of data: 1D signals of the form Eq (1), and 2D complex MRI k-space data.

Section 2 provided a mathematical investigation of the local self-similarity of signals of the form Eq (1). Signals of this form were found to be self-similar, and partitioned blocks of the signal may be *predicted exactly with multi-parent*

transforms; a consequence of Prony's method and AR modeling. One dimensional noiseless MRI k-space signals can be can be put into this form by using the boxcar model, thereby allowing the data to posses local self-similarity.

Section 3 provided an empirical study of the self-similarity of 2D complex Fourier data. Single and multi-parent transforms with complex fractal parameters were used to approximate Fourier domain blocks. Added noise decreased the self-similarity of the data, suggesting that fractal methods can find and utilize self-similar structures present in raw Fourier data. Use of an α term and multi-parent transforms improved the collage error, suggesting that fractal based techniques is able to uncover k-space self-similarity. The use of domain block isometries (or geometric maps), overlapping domain blocks, and other standard fractal techniques [6] should further improve our results.

Establishing connections between fractal and AR modeling theory provides new avenues for future investigation. Further relationships between fractal, AR, and physical parameters can be made. Ultimately however, concepts established in this paper are part of our overall research programme to use self-similarity to perform k-space extrapolation. Extension of mathematical results from Section 2 into two dimensions and use of multi-parent fractal techniques explored Section 3 may enable new approaches to the extrapolation of Fourier data, thereby providing a means of spatial domain resolution enhancement.

Acknowledgements

This research was supported in part by the Natural Sciences and Engineering Research Council of Canada (NSERC) in the form of a Discovery Grant (ERV) and a Postgraduate Scholarship (GSM), which are hereby gratefully acknowledged. We would also like to thank Drs. H. Peemoeller and C. Lemaire, Department of Physics, University of Waterloo, for helpful conversations and for providing us with MRI data. The data was obtained from a Bruker micro-magnetic resonance imaging spectrometer at UW which was purchased with funds provided by the Canada Foundation of Innovation (CFI) and the Ontario Innovation Trust. This project has been funded in part by the NSERC Strategic Grant, "Fusion and Analysis of Multiscale MRI and SEM Imaging Data of Porous Media".

References

1. Alexander, S.K.: Multiscale methods in image modeling and image processing, Ph.D. Thesis, Dept. of Applied Mathematics, University of Waterloo (2005)
2. Alexander, S.K., Vrscay, E.R., Tsurumi, S.: A simple model for affine self-similarity of images. In: ICIAR (submitted, 2008)
3. Buades, A., Coll, B., Morel, J.: A review of image denoising, with a new one. SIAM Multiscale Modeling & Simulation 4(2), 490–530 (2005)
4. Barbieri, M., Barone, P.: A two-dimensional Prony's method for spectral estimation. IEEE Transactions on Acous, Sp., and Sig. Proc. 40(11), 2747–2756 (1992)

5. Dabov, K., Foi, A., Katkovnik, V., Egiazarian, K.: Image denoising by sparse 3-D transform-domain collaborative filtering. IEEE Transactions Image Processing 16(8), 2080–2095 (2007)
6. Fisher, Y.: Fractal image compression. Springer, New York (1995)
7. Forte, B., Vrscay, E.: 1. Theory of generalized fractal transforms and 2. Inverse problem methods for generalized fractal transforms. In: Fisher, Y. (ed.) Fractal image encoding and analysis. NATO ASI Series F, vol. 159. Springer, NY (1998)
8. Ghazel, M.: Adaptive fractal and wavelet denoising, Ph.D. Thesis, Dept. of Applied Mathematics, University of Waterloo (2004)
9. Haacke, M., Liang, Z., Izen, S.: Constrained reconstruction: A superresolution, optimal signal-to-noise alternative to the Fourier transform in magnetic resonance imaging. Medical Physics 16(3), 388–397 (1989)
10. Haacke, M., Brown, R., Thompson, M., Venkatesan, R.: Magnetic resonance imaging: physical principles and sequence design. John Wiley & Sons, Inc., USA (1999)
11. Hinshaw, W., Lent, A.: An introduction to NMR imaging: from the Bloch equation to the imaging equation. Proceedings of the IEEE 71(3), 338–350 (1983)
12. Kumaresan, R., Tufts, D.: Estimating the parameters of exponentially damped sinusoids and pole-zero modeling in noise. IEEE Transactions on Acoustics, Speech, and Signal Processing 30(6), 833–840 (1982)
13. Liang, Z., Lauterbur, P.: Principles of magnetic resonance imaging, a signal processing perspective. IEEE Press, New York (2000)
14. Makhoul, J.: Linear prediction: a tutorial review. Proc. of the IEEE 63(4) (1975)
15. Mayer, G., Vrscay, E.: Iterated Fourier Transform Systems: A Method for Frequency Extrapolation. In: Kamel, M., Campilho, A. (eds.) ICIAR 2007. LNCS, vol. 4633, pp. 728–739. Springer, Heidelberg (2007)
16. Mayer, G., Vrscay, E.: Measuring information gain for frequency-encoded superresolution MRI. Magnetic Resonance Imaging 25(7), 1058–1069 (2007)
17. Prony, R.: Essai experimental et analytique. Paris J. de l'Ecole Poly. 1, 24–76 (1975)
18. Ranganath, S., Jain, A.: Two-dimensional linear prediction models – Part I: Spectral factorization and realization. IEEE Transactions on Acoustics, Speech, and Signal Processing 33(1), 280–299 (1985)
19. Vrscay, E.: A generalized class of fractal-wavelet transforms for image representation and compression. Can. J. Elect. & Comp. Eng. 23(1-2), 69–83 (1998)
20. Weiss, L., McDonough, R.: Prony's Method, Z-Transforms, and Pade Approximation. SIAM Review 5(2), 145–149 (1963)

Appendix: Relation between Fractal and AR Based Methods

Here we provide a short but key derivation of Eq (11). Using Eqs (6) and (7):

$$\begin{aligned}\mathbf{r} &= [r(0), r(1), r(2), ..., r(N_P - 1)] \\ &= [-\sum_{m=1}^{2N_C} a_m s(N_m), -\sum_{m=1}^{2N_c} a_m s(N_m + 1), \ldots, -\sum_{m=1}^{2N_c} a_m s(N_S - 1 - m)] \\ &= -\sum_{m=1}^{2N_C} a_m [s(N_m), s(N_m + 1), \ldots, s(N_S - 1 - m)] = -\sum_{m=1}^{2N_C} a_m \mathbf{d}_m\end{aligned}$$

where $N_m = N_S - N_P - m$.